RSC Advances

PAPER

View Article Online
View Journal | View Issue

Cite this: *RSC Adv.*, 2023, **13**, 19140

g-C_3N_4-modified Zr-Fc MOFs as a novel photocatalysis-self-Fenton system toward the direct hydroxylation of benzene to phenol†

Xu Jia,[a] Cong Liu,[a] Xuetong Xu,[a] Fuying Wang,[a] Weiwei Li,[a] Liuxue Zhang, *[a] Shuyan Jiao,*[a] Genxing Zhu[a] and Xiulian Wang[b]

Received 8th May 2023
Accepted 12th June 2023

DOI: 10.1039/d3ra03055e

rsc.li/rsc-advances

In order to explore a green, economic, and sustainable phenol production process, a heterojunction semiconductor materials g-C_3N_4/Zr-Fc MOF was synthesized *via* an *in situ* synthesis method. With the synergistic effect of photocatalysis and the Fenton effect, the composite could effectively catalyze the direct hydroxylation of benzene to phenol under visible light irradiation. The yield of phenol and the selectivity were 13.84% and 99.38% under the optimal conditions, respectively, and it could still maintain high photocatalytic activity after 5 photocatalytic cycles. Therefore, the designed photocatalysis-self-Fenton system has great potential in the field of the direct hydroxylation of benzene to phenol.

Introduction

Phenol is an important chemical intermediate in the industrial field. At present, it is mainly produced by the three-step isopropyl benzene process, which has serious limitations, such as dangerous intermediates and high energy consumption.[1] Therefore, a green, economic, and sustainable phenol production process is urgently needed. In recent years, the direct hydroxylation of benzene has attracted increasing attention. This is a mild, economically green solution.[2] Gu *et al.* achieved promising results with a phenol regimen using a light-induced benzene efficient hydroxylation, with high selectivity of up to 99% and good phenol yields.[3] Owing to its cost-effectiveness and environmental friendliness, photocatalysis could be applied as a competitive method to achieve benzene hydroxylation into phenols.

Recently, with the strong oxidation of hydroxyl radicals (·OH) the photocatalysis-self-Fenton process has been used by researchers to convert benzene into phenol.[4] The process of photo-Fenton mainly involves the transformation between Fe(III) and Fe(II).[5] Various iron-based MOFs have been used as photocatalyst for the direct hydroxylation of benzene to phenol. Xu proposed MIL-100(Fe) nanoparticles, which were synthesized by ethylene glycol with a uniform size and morphology to perform the photocatalytic direct hydroxylation of benzene experiments, and the result showed that the MIL-100(Fe) nanospheres possessed a good oxidation ability and high selectivity.[6] The experiments into phenol production with iron-based MOFs reported by Wang *et al.* also confirmed the feasibility of benzene–phenol conversion using the Fenton effect of the Fe-based MOFs, whereby the high catalytic activity of iron-containing materials in the selective oxidation process enables the wide application of Fe-based MOFs for the direct hydroxylation of benzene to produce phenol.[7] Owing to the tunable composition and structure of the iron-based MOF materials, they have great potential for the photocatalytic hydroxylation of benzene to produce phenol.[8,9] To obtain better photocatalytic phenol performance, the iron-based MOF structure can be adjusted to extend the photoresponse range. Constructing heterojunctions is a promising strategy to improve the performance of the heterogeneous photo-Fenton reaction (PFR).[10] As a photoresponse semiconductor, g-C_3N_4 has been often used to enhance the optical response range owing to its advantages of strong acid and alkali resistance, appropriate optical band range (2.76 eV), high thermal stability, and non-toxicity.[11–13] Zehra Durmus *et al.* built a unique hybrid structure between Ce-MOFs and g-C_3N_4 to improve the photocatalytic performance.[14] Devarayapalli *et al.* prepared g-C_3N_4/ZIF-67 heterojunction composites by a coupling cobalt–organic zeolite imidazole skeleton (ZIF-67) with g-C_3N_4 nanosheets synthesized by a simple microwave radiation method, which greatly improved the photocatalytic performance of the carbon nitride graphite.[15] Reza Abazari synthesized Ti-MIL-125-NH_2 modified with g-C_3N_4 by a simple-rapid ultrasonic method, which was then used as a visible-light photocatalyst with an improved photocatalytic performance.[16] All these experimental protocols demonstrated that the combination of g-C_3N_4 and iron-based MOFs would enhance the photocatalytic performance.

[a]*School of Materials and Chemical Engineering, Zhongyuan University of Technology, Zhengzhou, 450007, PR China. E-mail: zhanglx@zut.edu.cn; jiaosy@zut.edu.cn; Fax: +86-731-62506095; Tel: +86-731-62506699*

[b]*School of Energy and Environment, Zhongyuan University of Technology, Zhengzhou, 450007, PR China*

† Electronic supplementary information (ESI) available. See DOI: https://doi.org/10.1039/d3ra03055e

In this investigation, we report an efficient photocatalysis-self-Fenton system, namely g-C_3N_4/Zr-Fc MOF, constructed by an *in situ* composite method. Thereinto, zirconium(IV), 1,1′-ferrocenedicarboxylic acid, and g-C_3N_4 were selected as the central metal ion, organic ligand, and support system, respectively. Due to the synergistic effect of the mixed metals in MOFs, Zr-Fc MOFs can provide more abundant electrons and holes.[17–19] Besides, the heterojunction possesses a large specific surface area and stable structure. The hydroxyl radicals produced by the Fenton reaction between Fe(II) and hydrogen peroxide could have a synergistic effect with the presence of a bimetal to greatly improve the direct hydroxylation of benzene. At the same time, the band gap width of g-C_3N_4 is about 2.7 eV, which can effectively absorb sunlight and also it has a stable structure under light conditions.[20] Therefore, the designed photocatalyst was expected to possess a better effect in the direct hydroxylation of benzene to phenol under visible light.

Experimental

Materials and chemicals

1,1′-Ferrocenedicarboxylic acid (98%) was purchased from Sun Chemical Technology (Shanghai) Co., Ltd. Zirconium tetrachloride ($ZrCl_4$, 98%) was purchased from Guangdong Hachuring Chemical Reagent Co., Ltd. Melamine (99.5%) was purchased from Tianjin Guangfu Fine Chemical Research Institute. Acetic acid (AC) was purchased from Tianjin Tianli Chemical Reagent Co. Ltd. *N*-Dimethylformamide (AC) was purchased from Tianjin Fuyu Fine Chemical Co. Ltd. Benzene was purchased from Yantai Shuangshuang Chemical Co. Ltd. Ethanol (AC) was purchased from Tianjin Kermel Chemical Reagent Co., Ltd. Trifluoroacetic acid was purchased from Shanghai Macklin Biochemical Co., Ltd.

Synthesis of g-C_3N_4. An alumina crucible containing 10 g melamine was placed into a tubular furnace and heated to 600 °C at a heating rate of 2.3 °C min^{-1} under an air atmosphere and stabilized for 2 h. The yellow product in the crucible was carefully collected and ground into a powder. The prepared g-C_3N_4 powder was placed into an alumina crucible and annealed in an air stream at 550 °C at the rate of 2.3 °C min^{-1} for 3 h. The yellow-product layered g-C_3N_4 in the crucible was carefully collected.[21]

Synthesis of Zr-Fc MOFs. $ZrCl_4$ (700 mg, 3 mmol) and 1,1′-ferrocenedicarboxylic acid (823.2 mg, 3 mmol) were added in to 90 mL *N*,*N*′-dimethylformamide, and dispersed for 15 min in an ultrasonic cell dispersion apparatus. Then, glacial acetic acid (8.6 mL) was pipetted in to the mixture and stirred for about 15 min until the solution was uniform. The mixture was transferred into a 200 mL Teflon reactor and reacted at 120 °C for 12 h. Then, the product was collected by centrifugation, and washed with DMF and ethanol three times. The product was dried in a vacuum oven.[22]

Preparation and synthesis of g-C_3N_4/Zr-Fc MOFs. $ZrCl_4$ (700 mg, 3 mmol), 1,1′-ferrocenedicarboxylic acid (823.2 mg, 3 mmol), and g-C_3N_4 (0.2 g) were added in to 90 mL *N*,*N*′-dimethylformamide, and dispersed for 15 min in an ultrasonic cell dispersion apparatus. Then, glacial acetic acid (8.6 mL) was pipetted in to the mixture and stirred for about 15 min until the solution was uniform. The mixture was transferred into a 200 mL Teflon-lined reactor and reacted at 120 °C for 12 h. Then, the product was collected by centrifugation, and washed with DMF and ethanol three times. The product was dried in a vacuum oven.[22]

Characterization of the composite. The surface morphology and particle size of the samples were measured by scanning electron microscopy (SEM). The operating voltage was 10 k V. The silicon wafer containing the sample was fixed on the sample table with conductive tape, and then gold sputtering was applied. Finally, the sample was characterized by SEM. X-Ray diffraction spectroscopy was performed using an Ultima IV type X-ray diffraction instrument as the characterization instrument, with a nickel-filter Cu Kα target used as the incident light source, $\lambda = 0.15418$ nm as the incident wavelength, 5–80° as the scanning range, 40 kV as the scanning voltage, and 10° min^{-1} as the scanning speed. The crystal structure of the sample was obtained by X-ray diffraction spectrum analysis. The Fourier-transform infrared (FT-IR) information was investigated using a Nicolet iS50 system with measurements made at 4000–400 cm^{-1} as the detection range. The solid UV diffuse reflectance spectra were obtained through an integral sphere system equipped with a UV-2600 UV-visible spectrophotometer (Shimadzu, Japan). Barium sulfate powder was used as the reference to measure the baseline and then the DRS spectrum of the sample was determined.

Photocatalytic benzene hydroxylation experiments. The photocatalytic benzene direct hydroxylation experiments were carried out using the PCX-50C multi-channel photochemical reaction system (Beijing Perfectlight Technology Co., Ltd) as well as under visible-light irradiation. An LED lamp (5 W), which provided simulated sunlight full-spectrum irradiation (380–760 nm), was used as the light source. Benzene (1.6 mL), trifluoroacetic acid (0.1 g), and acetonitrile (11 mL) were added into the photoreactor. Then, the catalyst (20 mg) was added into the mixture and mixed evenly under magnetic stirring. The photocatalytic experiments were carried out at 60 °C, and hydrogen peroxide (0.6 mL) was added to the reactor within 30 min. The reaction was maintained for 4 h. After the reaction, the conversion of benzene and the yield of phenol were determined by gas chromatography (GC, Techcomp GC7900), for which the injection port temperature was 210 °C, FID was selected as the detector, and the temperature was set at 240 °C. To investigate the optimal reaction conditions for the experiments, the reaction conditions, such as the ratio of g-C_3N_4 and benzene, reaction time, and reaction temperature, were varied to explore the photocatalytic properties.

The conversion rate of benzene, selectivity of phenol, and yield of phenol were calculated using the following three formulas:

$$C\ (\text{conversion of benzene}) = 1 - \frac{\text{the mol of the residual benzene}}{\text{the mol of the initial benzene}} \times 100\%$$

$$S\ (\text{selectivity of phenol}) = \frac{\text{the mol of generated phenol}}{\text{the mol of invert benzene}} \times 100\%$$

$$Y\ (\text{yield of phenol}) = \frac{\text{the mol of generated phenol}}{\text{the mol of the initial benzene}} \times 100\%$$

Results and discussion

Sample structure characterization

The morphologies of g-C_3N_4, Zr-Fc MOF, and g-C_3N_4/Zr-Fc MOF were observed by SEM. As shown in Fig. 1, the prepared g-C_3N_4 with a large specific surface area possessed a sheet stacked structure with an irregular appearance and different sizes.[23] The Zr-Fc MOF possessed irregular sheet-like structures without agglomerates, which were consistent with previously reported SEM images.[24] The g-C_3N_4/Zr-Fc MOF was combined based on the g-C_3N_4 and Zr-Fc MOF. The Zr-Fc MOF particles were evenly dispersed over the g-C_3N_4, basically maintaining the original morphologies of g-C_3N_4 and Zr-Fc MOF, which indicated the successful composition of the g-C_3N_4/Zr-Fc MOF material (Fig. 1c).

The crystal structure of the sample as well as the crystallinity were investigated by X-ray diffraction, and the XRD profiles of g-C_3N_4, Zr-Fc MOF, and g-C_3N_4/Zr-Fc MOF are displayed in Fig. 2a. A strong diffraction peak occurring at 27.96° was the characteristic diffraction peak of the (002) crystal surface and corresponded to g-C_3N_4.[25] The characteristic diffraction peaks of the Zr-Fc MOF were consistent with the previously reported literature. The diffraction peaks at 2θ = 6.35°, 8.93°, 14.01°, 19.94°, and 25.82° could be observed from the XRD pattern of Zr-Fc MOF, corresponding to the (100), (110), (210), (310), and (320) crystal faces of Zr-Fc MOF, respectively.[26] The diffraction peaks of the g-C_3N_4/Zr-Fc MOF composites were consistent with the characteristic diffraction peaks of both g-C_3N_4 and Zr-Fc MOF, indicating that the g-C_3N_4/Zr-Fc MOF composites had been successfully prepared.

The structural information, such as chemical bonds and functional groups of g-C_3N_4, Zr-Fc MOF, and g-C_3N_4/Zr-Fc MOF, were acquired using the Fourier-transform infrared technique (Fig. 2b). For g-C_3N_4, the absorption peak at 813 cm^{-1} was attributed to the bending vibration peak of the triazine cycle in the g-C_3N_4 structure.[27] The absorption peak at 487 cm^{-1} was assigned to the asymmetric expansion vibration peak of Zr-(OC),while the absorption peaks that appeared at 794, 1027, 1107, and 1492 cm^{-1} were attributed to the out-of-plane deformation vibration of C–H, C–H deformation vibration, C–C deformation vibration, and C=C stretching vibration on the cyclopentadienyl ring.[28,29] This set of data suggested the formation of Zr-Fc MOF structures. The characteristic absorption peaks of ferrocene, Zr-(OC), and triazine cycle all appeared in the spectra of the composites, which indicated the successful preparation of the g-C_3N_4/Zr-Fc MOF.

To explore the photoresponse range of the sample and calculate the band gap width of the catalyst, characterization analysis was performed by solid ultraviolet-visible diffuse reflectance spectroscopy. As shown in Fig. 3a, the photoresponse range of Zr-Fc MOF was 250–400 nm, with two absorption peaks noted at 260 and 380 nm, respectively. However, when the Zr-Fc MOF was modified with g-C_3N_4, the photoresponse range of the Zr-Fc MOF was 250–400 nm with a red-shift. The band gap of semiconductors can be calculated according to the equation $(\alpha h\nu)^{1/n} = A(h\nu - E_g)$ (Fig. 3b). The band gap widths of g-C_3N_4, Zr-Fc MOF and g-C_3N_4/Zr-Fc MOF were 2.40, 2.13, and 2.03 eV, respectively. The band gap width of these semiconductors was gradually reduced, which indicated that the photocatalytic performance was gradually enhanced

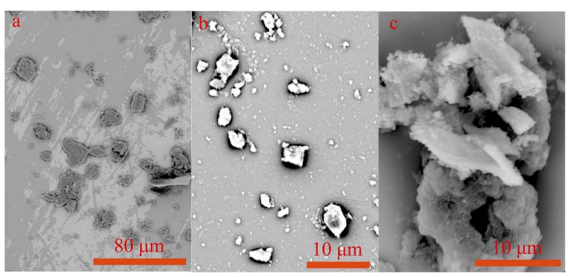

Fig. 1 SEM spectra of g-C_3N_4 (a), Zr-Fc MOF, (b) and g-C_3N_4/Zr-Fc MOF (c).

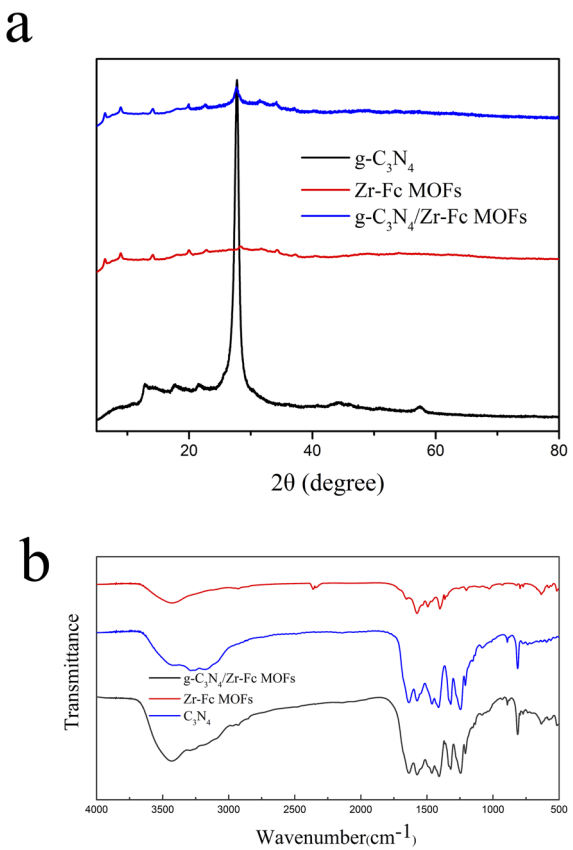

Fig. 2 XRD patterns (a) and infrared spectra (b) of g-C_3N_4, Zr-Fc MOF, and g-C_3N_4/Zr-Fc MOF.

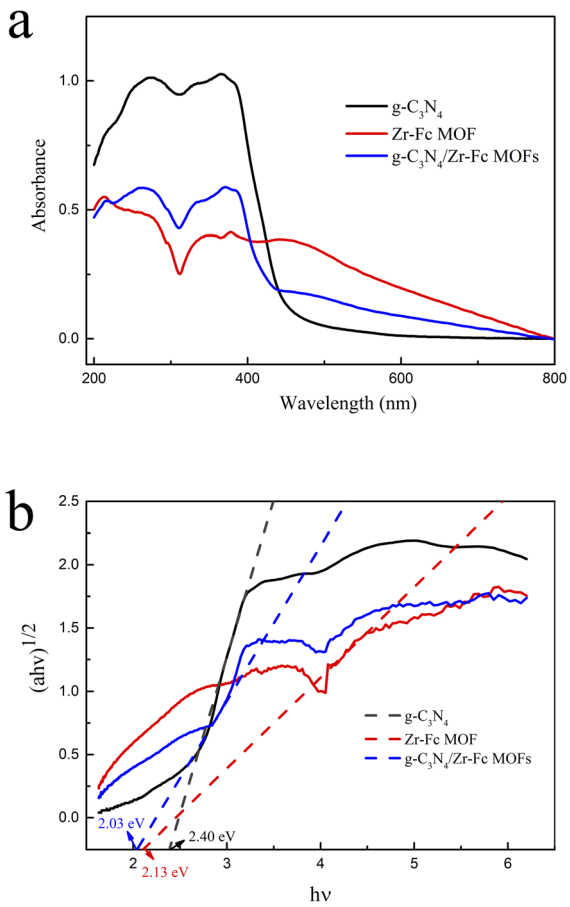

Fig. 3 Solid UV diffuse reflection (a) and band gap diagram (c) of g-C_3N_4, Zr-Fc MOF, and g-C_3N_4/Zr-Fc MOF.

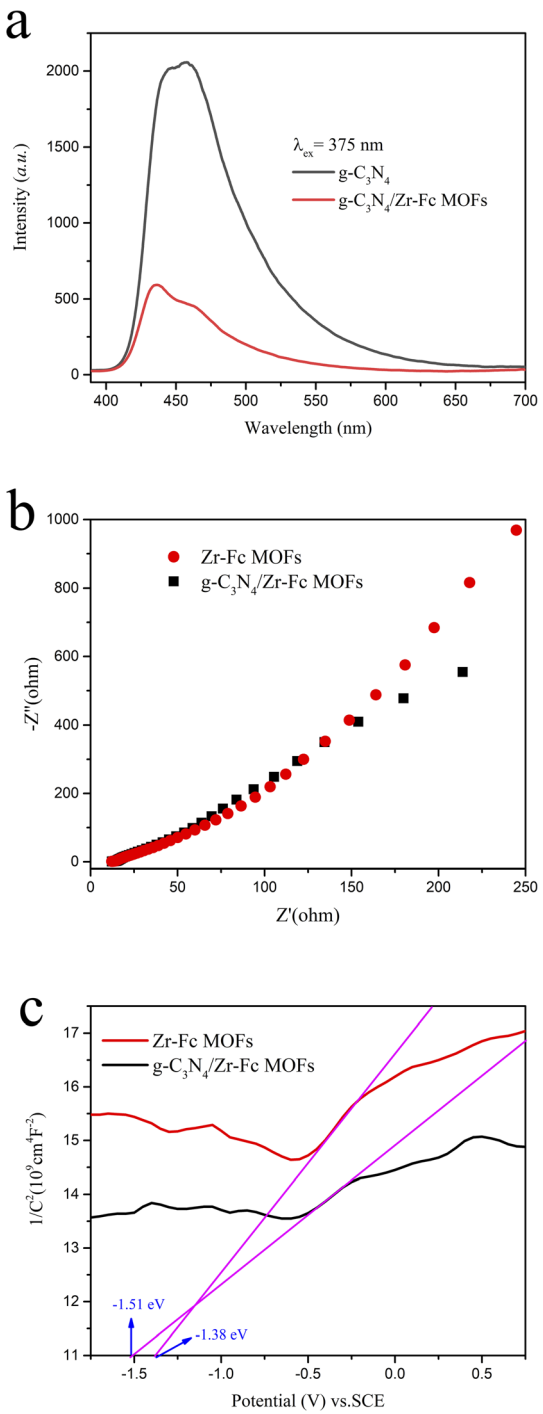

Fig. 4 PL profiles (a) of g-C_3N_4 and g-C_3N_4/Zr-Fc MOF. Electrochemical impedance profiles (b) and Mott–Schottky diagram (c) of Zr-Fc MOF and g-C_3N_4/Zr-Fc MOF.

under visible light. Hence, the g-C_3N_4/Zr-Fc MOF might be a desired photocatalyst for benzene hydroxylation to produce phenol.

The photogenerated hole–charge separation effect is a key factor in the photocatalytic organic oxidation reaction, whereby the higher the separation efficiency, the stronger the photocatalytic activity. Therefore, the photoluminescence performances of g-C_3N_4 and g-C_3N_4/Zr-Fc MOF were investigated at the emission wavelength of 375 nm (Fig. 4a). Compared to g-C_3N_4, the composite g-C_3N_4/Zr-Fc MOF displayed a lower fluorescence intensity at the wavelength of 440 nm. This phenomenon suggested that the g-C_3N_4/Zr-Fc MOF possessed a higher photogenerated hole–charge separation efficiency.

The effect of photogenerated charge–hole recombination could be further observed by electrochemical impedance spectroscopy. The EIS Nyquist curves of Zr-Fc MOF and g-C_3N_4/Zr-Fc MOF electrodes were detected under light avoidance conditions (Fig. 4b). When g-C_3N_4 was introduced to Zr-Fc MOF, the g-C_3N_4/Zr-Fc MOF showed a smaller radius of the Nyquist circle and smaller transfer resistance, which implied the composite possessed a lower recombination rate of photogenerated carriers. By fitting calculations, the charge-transfer resistance (R_{ct}) and solution resistance (R_s) of the g-C_3N_4/Zr-Fc MOF were calculated to be 6.97 and 9.39 Ω, respectively. The charge-transfer resistance (R_{ct}) and solution resistance (R_s) of Zr-Fc MOF were 38.33 and 96.16 Ω, respectively. Hence, the g-C_3N_4/Zr-Fc MOF displayed a higher photocatalytic performance.

The information of the semiconductor type and flat band potential could be obtained *via* Mott–Schottky curves. In order to investigate the effect of g-C_3N_4 introduction to Zr-Fc MOF on the band structure, Mott–Schottky curves of Zr-Fc MOF and g-

C_3N_4/Zr-Fc MOF semiconductors were obtained by the Mott–Schottky measurement method (Fig. 4c). The two curves revealed that the tangent line presented a positive slope at the frequency of 1000 Hz, which indicated that the Zr-Fc MOF and g-C_3N_4/Zr-Fc MOF were both typical N-type semiconductors. Further analysis showed that the flat band potential of the Zr-Fc MOF and g-C_3N_4/Zr-Fc MOF were about −1.38 and −1.51 V, respectively. Previous studies have reported that the conduction band (CB) potential of N-type semiconductors is negative 0.1 V compared with its flat band potential.[30] It could be found that g-C_3N_4/Zr-Fc MOF had a more negative conduction band potential than Zr-Fc MOF, which demonstrated that the incorporation of g-C_3N_4 was valuable for the improvement of the photogenerated charge–hole separation efficiency. In conclusion, as the composite rate of the photocharged holes could be effectively suppressed, the photocarrier lifetime could be extended, and the photoelectrons could be effectively transferred to produce active free radicals, which could be applied for the photocatalytic benzene hydroxylation reaction.

Photocatalytic experiments

Effect of different catalysts. The enhancement of the photocatalytic performance was estimated by comparing the ability of the three photocatalytic materials for the direct hydroxylation of benzene under visible light. As shown in Table 1, a lower phenol yield could be detected in the post-reaction products catalyzed by g-C_3N_4 and Zr-Fc MOF, whereby the phenol yields were 4.78% and 8.80%, respectively. When the composite was prepared by the combination of g-C_3N_4 and Zr-Fc MOF, the yield was increased to 13.84%, and the selectivity was 99.38% when using the g-C_3N_4/Zr-Fc MOF as the catalyst under the same conditions. This might be due to the g-C_3N_4 having a photocatalytic ability, while the Zr-Fc MOF could activate hydrogen peroxide to generate free radicals (˙OH) *via* a Fenton reaction, and then the synergistic effect of photocatalysis and the Fenton reaction improved the direct hydroxylation of benzene to phenol. Therefore, in subsequent research experiments, the g-C_3N_4/Zr-Fc MOF was selected as the photocatalyst for benzene hydroxylation to phenol.

Effect of the catalyst dosage. In order to explore the effect of the quality of the as-prepared g-C_3N_4/Zr-Fc MOF on the benzene hydroxylation to phenol performance, catalyst samples of different amounts were investigated under the photocatalytic process. As displayed in Table 2, when there was no photocatalyst, it was hard for benzene to directly undergo hydroxylation under light irradiation, and only a little phenol was produced. With the increase in the photocatalyst amount, the performance of the benzene hydroxylation reaction was greatly improved, mainly because more catalysts could meet the quantity of Fe^{2+} demanded for the Fenton reaction, and more ·OH was generated to react with benzene to produce phenol.[31,32] When the catalyst quality was further increased, the yield of phenol decreased instead. This might be due to the increased catalyst powder in the photocatalytic process, which might cause a shielding effect of light while the excess hydroxyl radicals could not participate in the reaction in time due to their short life. Therefore, considering all the above, the optimal catalyst mass was 20 mg.

Effect of the amount of H_2O_2. The amount of H_2O_2 is another vital factor in the direct hydroxylation of benzene under the photocatalysis. Hence, the amount of H_2O_2 was investigated to explore the appropriate conditions for the reaction. As illustrated in Table 3, the photocatalyst could obtain a better benzene hydroxylation to phenol performance, whereby the phenol yield and selectivity were 13.84% and 99.38%, respectively, under the volume ratio of $n(H_2O_2)/n(\text{benzene}) = 8:3$. However, when the amount of H_2O_2 was increased, the yield of phenol, the conversion rate of benzene, and the selectivity of phenol gradually decreased. This might be due to the H_2O_2 undergoing a self-decomposition during the reaction, and the self-decomposition rate was faster than that of benzene hydroxylation, which would cause the reaction solution to gradually become two phases, thus hindering the interaction

Table 1 Effect of different catalysts on catalytic benzene hydroxylation[a]

Sample	Yield (%)	Conversion (%)	Selectivity (%)
g-C_3N_4	4.78	4.92	97.15
Zr-Fc MOF	8.80	8.95	98.32
g-C_3N_4/Zr-Fc MOF	13.84	13.93	99.38

[a] Reaction conditions: catalyst (1.5 mg mL^{-1}), benzene (1.6 mL, 18.05 mmol), H_2O_2 (30 wt%) (0.6 mL), acetonitrile (11 mL), trifluoroacetic acid (0.1 g), time: 4 h, and *T*: 333 K.

Table 2 Effect of the amount of catalyst on catalytic benzene hydroxylation[a]

Entry	*m* (mg mL^{-1})	Yield (%)	Conversion (%)	Selectivity (%)
1	0	4.87	5.03	96.81
2	0.75	7.69	7.96	96.61
3	1.50	13.84	13.93	99.38
4	2.25	8.48	8.85	95.82

[a] Reaction conditions: benzene (1.6 mL, 18.05 mmol), H_2O_2 (30 wt%) (0.6 mL), acetonitrile (11 mL), trifluoroacetic acid (0.1 g), time: 4 h, and *T*: 333 K.

Table 3 Effect of the added amount of H_2O_2 on catalytic benzene hydroxylation[a]

Entry	$n(H_2O_2)/n$(benzene)	Yield (%)	Conversion (%)	Selectivity (%)
1	2/8	7.39	7.57	97.62
2	3/8	13.84	13.93	99.38
3	4/8	9.85	9.98	98.70
4	5/8	8.66	8.80	98.40
5[b]	3/8	8.17	8.28	98.67

[a] Reaction conditions: catalyst (1.5 mg mL^{-1}), benzene (1.6 mL, 18.05 mmol), acetonitrile (11 mL), trifluoroacetic acid (0.1 g), time: 4 h, and *T*: 333 K. [b] No visible-light exposure.

between benzene and the catalyst.[33] Furthermore, the effect of light on benzene hydroxylation to produce phenol was also explored under the same reaction conditions with the volume ratio of $n(H_2O_2)/n(\text{benzene}) = 8:3$. When there was no visible-light irradiation, the yield of phenol was 8.17%, which implied that only the Fenton reaction occurred under dark conditions. Hence, the Fenton reaction and photocatalysis cooperate to improve the benzene hydroxylation to phenol performance.

Effect of trifluoroacetic acid dosage. As a cocatalyst, trifluoroacetic acid plays a key role in the direct hydroxylation of benzene, whereby it can enhance the activity of the ferrous ions in g-C_3N_4/Zr-Fc MOF.[34] As displayed in Table 4, when the cocatalyst was not added into the photocatalytic process, the yield of phenol was only 6.27%. With the increase in trifluoroacetic acid, the yield of phenol gradually increased. When the addition of trifluoroacetic acid reached 0.1 g, the result of the reaction was optimal, and the phenol yield, benzene conversion rate, and selectivity were 13.84%, 13.93%, and 99.38%. However, when the amount of trifluoroacetic acid was further increased, the photocatalytic performance declined. This might be due to the presence of trifluoroacetic acid inhibiting the occurrence of peroxidation reactions, so the more trifluoroacetic acid, the stronger the inhibition, and the smaller the phenol yield. The effects of other acidic additives were studied when used in place of trifluoroacetic acid, including acetic acid, formic acid, hydrochloric acid, and phosphoric acid. The results showed that trifluoroacetic acid had the best co-catalytic effect among these acids (Fig. S6†).

Effect of the reaction time and temperature. The effect of different reaction times on the selective catalytic oxidation of benzene by g-C_3N_4/Zr-Fc MOF is illustrated in Table 5. The reaction time plays a vital role in the direct hydroxylation of benzene to phenol, whereby initially the yield increased with the increase in reaction time, and then the yield decreased as the time was further increased. The yield of phenol reached to 13.84%, when the reaction time was 4 h. Later, the photocatalytic activity decreased slightly with the extension of reaction time, which might be due to some peroxidation reactions of phenol and hydroxyl groups occurring to produce benzoquinone byproducts with the increase in reaction time.

The effect of different reaction temperatures on the selective catalytic oxidation of benzene by g-C_3N_4/Zr-Fc MOF is illustrated in Table 6. Initially the yield increased with the increase in reaction time, and then the yield decreased as the time was further increased. The ideal benzene conversion and phenol selectivity were obtained at 60 °C. The reason for this might be because the higher reaction temperature was conducive to the generation of active free radicals required in the photocatalytic process, which accelerated the photocatalytic reaction and increased the benzene conversion and yield of phenol to 13.84% and 13.93%, respectively. When the reaction temperature was raised close to the boiling point of benzene, the volatilization of the reactants was easier.[35] Also, the self-decomposition of hydrogen peroxide and the deep oxidation of phenol might be caused by high temperature. Therefore, the optimum time for benzene hydroxylation was 4 h and the optimum temperature was 60 °C.

For the catalyst, its regeneration and reusability are also an important factor to be investigated. Thus here, after each photocatalytic reaction, the composite was collected by centrifugation and washed with ethanol, as shown in Fig. 5, the photocatalytic performance of g-C_3N_4/Zr-Fc MOF could be well maintained after five cycles, and the yield of phenol and the selectivity were 12.49% and 94.88%, respectively. This suggested that the semiconductor photocatalyst was relatively stable and could achieve the goal of being recycled and reused.

A comparative study of g-C_3N_4/Zr-Fc MOF and other photocatalysts previously reported for the photocatalytic hydroxylation of benzene to phenol was conducted, and the results are shown in Table 7. The phenol selectivity (99%) and yield (13.84%) obtained using the g-C_3N_4/Zr-Fc MOF photocatalyst were higher than or comparable with those obtained using other photocatalysts.

Table 4 Effect of the amount of trifluoroacetic acid on catalytic benzene hydroxylation[a]

Entry	Mass of TFA (g)	Yield (%)	Conversion (%)	Selectivity (%)
1	0	6.27	6.52	96.16
2	0.05	7.45	7.79	95.64
3	0.10	13.84	13.93	99.38
4	0.15	10.86	11.23	96.71
5	0.20	7.96	8.03	99.13

[a] Reaction conditions: catalyst (1.5 mg mL^{-1}), benzene (1.6 mL, 18.05 mmol), H_2O_2 (30 wt%) (0.6 mL), acetonitrile (11 mL), time: 4 h, and T: 333 K.

Table 5 Effect of the reaction time on catalytic benzene hydroxylation[a]

Entry	t (h)	Yield (%)	Conversion (%)	Selectivity (%)
1	3	9.53	10.06	94.73
2	4	13.84	13.93	99.38
3	5	10.61	11.37	93.31

[a] Reaction conditions: catalyst (1.5 mg mL^{-1}), benzene (1.6 mL, 18.05 mmol), H_2O_2 (30 wt%) (0.6 mL), acetonitrile (11 mL), trifluoroacetic acid (0.1 g), and T: 333 K.

Table 6 Effects of the reaction temperature on catalytic benzene hydroxylation[a]

Entry	T (°C)	Yield (%)	Conversion (%)	Selectivity (%)
1	50	9.30	9.64	96.47
2	60	13.84	13.93	99.38
3	70	5.22	5.39	96.85

[a] Reaction conditions: catalyst (1.5 mg mL^{-1}), benzene (1.6 mL, 18.05 mmol), H_2O_2 (30 wt%) (0.6 mL), acetonitrile (11 mL), trifluoroacetic acid (0.1 g), and time: 4 h.

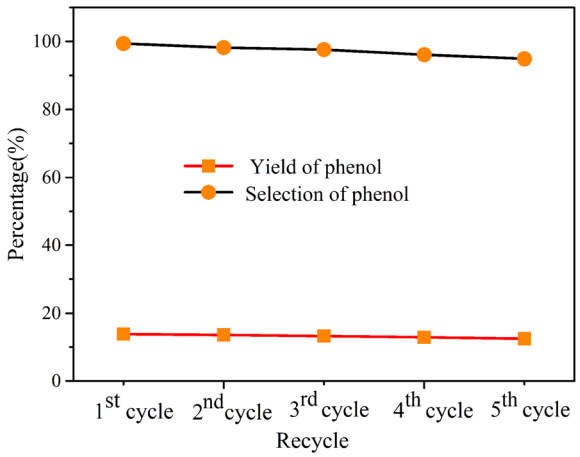

Fig. 5 Regeneration and reusability of g-C_3N_4/Zr-Fc MOF. Reaction conditions: catalyst (1.5 mg mL^{-1}), benzene (1.6 mL, 18.05 mmol), H_2O_2 (30 wt%) (0.6 mL), acetonitrile (11 mL), trifluoroacetic acid (0.1 g), time: 4 h, and $T = 333$ K.

Table 7 Comparison of the photocatalytic activity of g-C_3N_4/Zr-Fc MOF with other reported photocatalysts for the photocatalytic hydroxylation of benzene to phenol

Sample	Amount	Time (h)	Yield (%)	Ref.
Fe–Cu/beta	5 mg mL^{-1}	6	10.5	36
Fe–g-C_3N_4/SBA-15	5.5 mg mL^{-1}	4	11.9	37
Fe–g-C_3N_4	5.5 mg mL^{-1}	4	8.3	38
UiO-66-NH_2-SA-V	1.5 mg mL^{-1}	4	15.3	39
5% Cr–CdS/ZnO	5 mg mL^{-1}	4	11.1	40
g-C_3N_4/Zr-Fc MOFs	1.5 mg mL^{-1}	4	13.84	This work

The h^+, e^-, and ·OH were the main active substances involved in the photocatalytic reaction.[41] In order to illuminate the mechanism of g-C_3N_4/Zr-Fc MOF in the process of the direct

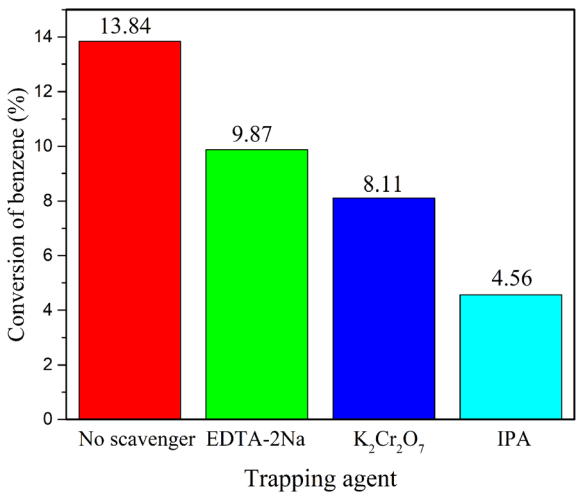

Fig. 6 Free-radical-trapping experiments. Reaction conditions: catalyst (1.5 mg mL^{-1}), benzene (1.6 mL, 18.05 mmol), H_2O_2 (30 wt%) (0.6 mL), solvent (acetonitrile: 11 mL), trifluoroacetic acid (0.1 g), $t = 4$ h, and $T = 333$ K.

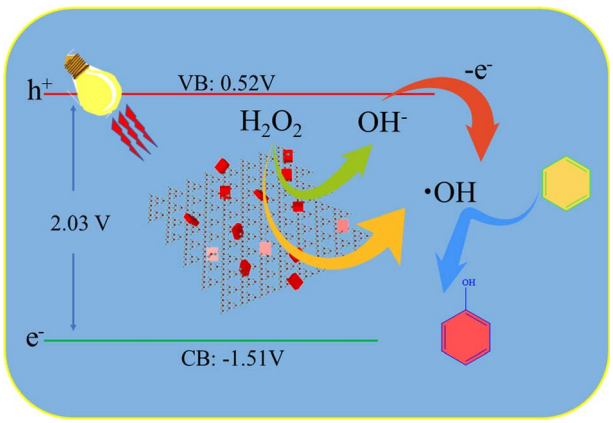

Fig. 7 Schematic diagram of the proposed photocatalytic mechanism.

hydroxylation of benzene to phenol under photocatalysis, the active substances that played a vital role in the reaction were determined by free-radical-capture experiments under the optimal conditions. Thereinto, isopropanol (IPA), potassium dichromate ($K_2Cr_2O_7$), and disodium ethylenediaminetetraacetate (EDTA-2Na) were selected as scavengers of hydroxyl radicals (·OH), electrons (e^-), and holes (h^+), respectively. As shown in Fig. 6, when the capture agents were added into the reaction mixture, the yield of phenol decreased to some extent in all cases. Thereinto, the yield of phenol was greatly inhibited with the addition of IPA. This phenomenon implied that the direct hydroxylation of benzene to phenol was primarily driven by the participation of hydroxyl radicals.

Basic reaction mechanism

According to the aforementioned free-radical-trapping experiment results, a possible photocatalytic mechanism of benzene hydroxylation to phenol is proposed in Fig. 7. In the visible-irradiated Fenton system, electrons and holes are mainly generated from the semiconductor g-C_3N_4/Zr-Fc MOF under visible light, and hydroxyl radicals (·OH) are primarily produced by the Fenton reaction, in which hydrogen peroxide is reduced by Fe^{2+} in the photocatalyst. Furthermore, ·OH also could be generated by the interaction between hydrogen peroxide, electrons, and holes. First, the H_2O_2 reacts with electrons to produce OH^-, and then, the generated OH^- could be oxidized by h^+ to give ·OH. All the obtained ·OH could then oxidize benzene molecules to phenol.[42,43]

Conclusions

In summary, a novel photocatalytic semiconductor material g-C_3N_4/Zr-Fc MOFs was successfully prepared *via* an *in situ* synthesis method. Compared with g-C_3N_4 and Zr-Fc MOF, the photocatalytic performance of the composite was significantly improved, and it could effectively catalyze the direct hydroxylation of benzene to phenol under visible-light irradiation. The yield of phenol and selectivity were 13.84% and 99.38% under the optimal conditions, respectively. The performance and

structure of the catalyst were relatively stable, and it could still maintain high photocatalytic activity after 5 photocatalytic cycles. Based on these excellent properties, the g-C_3N_4/Zr-Fc MOF can be expected to be widely used in the field of photocatalytic benzene direct hydroxylation to phenol.

Conflicts of interest

There are no conflicts to declare.

Acknowledgements

This project was financially supported by 2018 Funding Plan for Young Core Teachers of Zhongyuan University of Technology, Discipline Strength Improvement Program of Zhongyuan University of Technology: Program for Cultivating Disciplinary Young Master Supervisor (SD202204), the Basic Scientific Research Program of Zhongyuan University of Technology (K2018QN018).

Notes and references

1 W. Han, W. Xiang, J. Shi, *et al.*, Recent advances in the heterogeneous photocatalytic hydroxylation of benzene to phenol, *Molecules*, 2022, **27**(17), 5457.
2 S. M. Hosseini, M. Ghiaci, S. A. Kulinich, *et al.*, Au-Pd@g-C_3N_4 as an efficient photocatalyst for visible-light oxidation of benzene to phenol: experimental and mechanistic study, *J. Phys. Chem. C*, 2018, **122**(48), 27477–27485.
3 Y. Gu, Q. Li, D. Zang, *et al.*, Light-induced efficient hydroxylation of benzene to phenol by quinolinium and polyoxovanadate-based supramolecular catalysts, *Angew. Chem., Int. Ed.*, 2021, **60**(24), 13310–13316.
4 R. Liu, Y. Xu and B. Chen, Self-assembled nano-FeO(OH)/reduced graphene oxide aerogel as a reusable catalyst for photo-Fenton degradation of phenolic organics, *Environ. Sci. Technol.*, 2018, **52**(12), 7043–7053.
5 W. Q. Li, Y. X. Wang, J. Q. Chen, *et al.*, Boosting photo-Fenton process enabled by ligand-to-cluster charge transfer excitations in iron-based metal organic framework, *Appl. Catal., B*, 2022, **302**, 120882.
6 B. Xu, Z. Chen, B. Han, *et al.*, Glycol assisted synthesis of MIL-100(Fe) nanospheres for photocatalytic oxidation of benzene to phenol, *Catal. Commun.*, 2017, **98**, 112–115.
7 D. Wang, M. Wang and Z. Li, Fe-based metal–organic frameworks for highly selective photocatalytic benzene hydroxylation to phenol, *ACS Catal.*, 2015, **5**(11), 6852–6857.
8 B. L. Xiang, L. Fu, Y. Li, *et al.*, Preparation of Fe(II)/MOF-5 catalyst for highly selective catalytic hydroxylation of phenol by equivalent loading at room temperature, *J. Chem.*, 2019, **2019**, 1–10.
9 Q. Zhao, L. Zhang, M. Zhao, *et al.*, Vanadium oxyacetylacetonate grated on metal organic framework as catalyst for the direct hydroxylation of benzene to phenol, *ChemistrySelect*, 2020, **5**(22), 6818–6822.
10 D. Wang and Z. Li, Iron-based metal–organic frameworks (MOFs) for visible-light-induced photocatalysis, *Res. Chem. Intermed.*, 2017, **43**, 5169–5186.
11 X. Wang, S. Blechert and M. Antonietti, Polymeric graphitic carbon nitride for heterogeneous photocatalysis, *ACS Catal.*, 2012, **2**(8), 1596–1606.
12 S. Cao, J. Low, J. Yu, *et al.*, Polymeric photocatalysts based on graphitic carbon nitride, *Adv. Mater.*, 2015, **27**(13), 2150–2176.
13 J. Liu, H. Wang and M. Antonietti, Graphitic carbon nitride "reloaded": emerging applications beyond (photo) catalysis, *Chem. Soc. Rev.*, 2016, **45**(8), 2308–2326.
14 Z. Durmus, R. Köferstein, T. Lindenberg, *et al.*, Preparation and characterization of Ce-MOF/g-C_3N_4 composites and evaluation of their photocatalytic performance, *Ceram. Int.*, 2023, **49**, 24428–24441.
15 K. C. Devarayapalli, S. V. P. Vattikuti, T. V. M. Sreekanth, *et al.*, Hydrogen production and photocatalytic activity of g-C_3N_4/Co-MOF (ZIF-67) nanocomposite under visible light irradiation, *Appl. Organomet. Chem.*, 2020, **34**(3), e5376.
16 R. Abazari, A. R. Mahjoub and G. Salehi, Preparation of amine functionalized g-C_3N_4@ H/SMOF NCs with visible light photocatalytic characteristic for 4-nitrophenol degradation from aqueous solution, *J. Hazard. Mater.*, 2019, **365**, 921–931.
17 P. Xiao, R. Osuga, Y. Wang, *et al.*, Bimetallic Fe–Cu/beta zeolite catalysts for direct hydroxylation of benzene to phenol: effect of the sequence of ion exchange for Fe and Cu cations, *Catal. Sci. Technol.*, 2020, **10**(20), 6977–6986.
18 Y. Wu, X. Zhang, F. Wang, *et al.*, Synergistic effect between Fe and Cu species on mesoporous silica for hydroxylation of benzene to phenol, *Ind. Eng. Chem. Res.*, 2021, **60**(23), 8386–8395.
19 L. Zeng, H. Liang, P. An, *et al.*, Carbon encapsulated bimetallic FeCo nanoalloys for one-step hydroxylation of benzene to phenol, *Appl. Catal., A*, 2022, **633**, 118499.
20 M. Garrido, M. Barrejón, J. A. Berrocal, *et al.*, Polyaromatic cores for the exfoliation of popular 2D materials, *Nanoscale*, 2022, **14**(25), 8986–8994.
21 J. Du, S. Li, Z. Du, *et al.*, Boron/oxygen-codoped graphitic carbon nitride nanomesh for efficient photocatalytic hydrogen evolution, *Chem. Eng. J.*, 2021, **407**, 127114.
22 X. Ma, Z. Deng, Z. Li, *et al.*, A photothermal and Fenton active MOF-based membrane for high-efficiency solar water evaporation and clean water production, *J. Mater. Chem. A*, 2020, **8**(43), 22728–22735.
23 W. Yan, L. Yan and C. Jing, Impact of doped metals on urea-derived g-C_3N_4 for photocatalytic degradation of antibiotics: structure, photoactivity and degradation mechanisms, *Appl. Catal., B*, 2019, **244**, 475–485.
24 Z. Deng, H. Yu, L. Wang, *et al.*, Ferrocene-based metal-organic framework nanosheets loaded with palladium as a super-high active hydrogenation catalyst, *J. Mater. Chem. A*, 2019, **7**(26), 15975–15980.
25 X. Wang, F. Wang, C. Bo, *et al.*, Promotion of phenol photodecomposition and the corresponding

decomposition mechanism over g-C_3N_4/TiO_2 nanocomposites, *Appl. Surf. Sci.*, 2018, **453**, 320–329.

26 Z. Deng, T. Wan, D. Chen, *et al.*, Photothermal-Responsive Microporous Nanosheets Confined Ionic Liquid for Efficient CO_2 Separation, *Small*, 2020, **16**(34), 2002699.

27 M. Lu, Z. Pei, S. Weng, *et al.*, Constructing atomic layer g-C_3N_4-CdS nanoheterojunctions with efficiently enhanced visible light photocatalytic activity, *Phys. Chem. Chem. Phys.*, 2014, **16**(39), 21280–21288.

28 B. Van de Voorde, I. Stassen, B. Bueken, *et al.*, Improving the mechanical stability of zirconium-based metal–organic frameworks by incorporation of acidic modulators, *J. Mater. Chem. A*, 2015, **3**(4), 1737–1742.

29 J. Shimei and W. Yue, Vibrational spectra of an open ferrocene and a half-open ferrocene, *Spectrochim. Acta, Part A*, 1999, **55**(5), 1025–1033.

30 S. Samanta, R. Yadav, A. Kumar, *et al.*, Surface modified C, O co-doped polymeric g-C_3N_4 as an efficient photocatalyst for visible light assisted CO_2 reduction and H_2O_2 production, *Appl. Catal., B*, 2019, **259**, 118054.

31 X. Wei, N. Zhu, X. Huang, *et al.*, Efficient degradation of sodium diclofenac *via* heterogeneous Fenton reaction boosted by Pd/Fe@Fe_3O_4 nanoparticles derived from bio-recovered palladium, *J. Environ. Manage.*, 2020, **260**, 110072.

32 P. P. Xu, L. Zhang, X. Jia, *et al.*, A novel heterogeneous catalyst NH_2-MIL-88/$PMo_{10}V_2$ for the photocatalytic activity enhancement of benzene hydroxylation, *Catal. Sci. Technol.*, 2021, **11**(19), 6507–6515.

33 Y. Fang, L. Zhang, Q. Zhao, *et al.*, Highly selective visible-light photocatalytic benzene hydroxylation to phenol using a new heterogeneous photocatalyst UiO-66-NH_2-SA-V, *Catal. Lett.*, 2019, **149**, 2408–2414.

34 G. Grigoropoulou, J. H. Clark and J. A. Elings, Recent developments on the epoxidation of alkenes using hydrogen peroxide as an oxidant, *Green Chem.*, 2003, **5**(1), 1–7.

35 S. Farahmand, M. Ghiaci and S. Asghari, Oxo-vanadium(IV) phthalocyanine implanted onto the modified SBA-15 as a catalyst for direct hydroxylation of benzene to phenol in acetonitrile-water medium: A kinetic study, *Chem. Eng. Sci.*, 2021, **232**, 116331.

36 P. Xiao, Y. Wang, J. N. Kondo, *et al.*, Iron-and copper-exchanged Beta zeolite catalysts for hydroxylation of benzene to phenol with H_2O_2, *Chem. Lett.*, 2018, **47**(9), 1112–1115.

37 X. Chen, J. Zhang, X. Fu, *et al.*, Fe-g-C_3N_4-catalyzed oxidation of benzene to phenol using hydrogen peroxide and visible light, *J. Am. Chem. Soc.*, 2009, **131**(33), 11658–11659.

38 Z. Ding, X. Chen, M. Antonietti, *et al.*, Synthesis of transition metal-modified carbon nitride polymers for selective hydrocarbon oxidation, *ChemSusChem*, 2011, **4**(2), 274–281.

39 Y. Fang, L. Zhang, Q. Zhao, *et al.*, Highly Selective Visible-Light Photocatalytic Benzene Hydroxylation to Phenol Using a New Heterogeneous Photocatalyst UiO-66-NH_2-SA-V, *Catal. Lett.*, 2019, **149**, 2408–2414.

40 W. Han, W. Xiang, Z. Meng, *et al.*, A novel Cr-doped CdS/ZnO nanocomposite for efficient photocatalytic hydroxylation of benzene to phenol, *Colloids Surf., A*, 2023, **670**, 131529.

41 B. Han, X. Li, Z. Zhang, *et al.*, A novel strategy to research the mechanism of rutile TiO_2 with excellent photocatalytic performance, *Nanotechnology*, 2021, **33**(3), 035704.

42 F. Zhu, S. Zhou, M. Sun, *et al.*, Heterogeneous activation of persulfate by Mg doped $Ni(OH)_2$ for efficient degradation of phenol, *Chemosphere*, 2021, 131647.

43 S. J. Feng, B. Yue, Y. Wang, *et al.*, Hydroxylation of benzene over V-HMS catalysts with the addition of Fe as the second metal component, *Acta Phys.-Chim. Sin.*, 2011, **27**(12), 2881–2886.